Ray tracing method for the grazing incidence flat-field imaging soft X-ray spectrometer*

Dong Quan-Li(董全力)[a)†], Liu Yun-Quan(刘运全)[b)], Teng Hao(腾 浩)[c)], Li Ying-Jun(李英骏)[d)], and Zhang Jie(张 杰)[c)e)]

[a)] *School of Physics and Optoelectronic Engineering, Ludong University, Yantai* 260405, *China*

[b)] *Department of Physics, State Key Laboratory for Mesoscopic Physics, Peking University, Beijing* 100871, *China, Collaborative Innovation Center of Quantum Matter, Beijing* 100871, *China*

[c)] *Beijing National Laboratory of Condensed Matter Physics, Institute of Physics, Chinese Academy of Sciences, Beijing* 100190, *China*

[d)] *State Key Laboratory for GeoMechanics and Deep Underground Engineering, China University of Mining and Technology, Beijing* 100083, *China*

[e)] *Key Laboratory for Laser Plasmas (MoE) and Department of Physics, Shanghai Jiao Tong University, Shanghai* 200240, *China*

(Received 9 December 2013; revised manuscript received 21 January 2014; published online 20 April 2014)

A ray tracing method is introduced for helping adjustment and spectra analysis of the grazing incidence flat-field imaging soft X-ray spectrometer. For a single point source, the spectra images obtained by separate components, the toroidal mirror, and the grazing incidence flat-field concave grating with varied line spaces are given respectively. The calculated spectral images of the single point source by the spectrometer are also given for comparison with measurements with different experimental alignments.

Keywords: flat-field grating spectrometer, soft X-ray diagnosis

PACS: 52.70.La, 42.82.Bq, 42.62.Fi, 42.55.Vc **DOI:** 10.1088/1674-1056/23/6/065206

1. Introduction

The spectroscopy technique is commonly used for the non-interruptive diagnosis of plasmas. For radiation with high photon energy, diffractive components of the diagnosis system are usually replaced by reflective ones with a grazing incidence for high reflection efficiency. The astigmatism inherited from the grazing incidence then has to be compensated for by using other components in front so that the sagittal image and the meridional image can be located at the same position.

The flat-field soft X-ray spectrometer is popularly used for the diagnosis of hot plasmas. It consists of a grazing incidence concave grating with variable line spaces, producing a flat spectral plane suitable to the electric detector, and a toroidal mirror in front of it for the astigmatism compensation besides the function of signal gathering. The abberations of the grating were formularized by Harada and Kita,[1] Chrisp,[2] and Li *et al.*,[3] and were used in the analysis of the characteristics of the flat-field XUV spectrograph system.[4] However, those formulas are mostly focused on analyzing the abberations of the images on the expected flat spectral plane. To align the grazing incidence flat-field spectrometer, it is necessary to have in mind the whole image and know the characteristics of the images on or near the imaging plane. The ray-tracing method can be applied to produce the images. In this paper, the formulas needed in the ray-tracing method are derived, and the images formed on or near the flat imaging plane are presented, then one can compare the spatially resolved spectral measurements obtained in the instrument alignments and experiments.

2. Configuration of the flat-field spectrometer

The structure of the flat-field soft X-ray spectrometer is simplified as schemed shown in Fig. 1. A soft X-ray signal is emitted from the object, reflected by the toroidal mirror, and then by the varied line-spacing grating, and finally forms a spectral image on the plane. The toroidal mirror with different radii in the meridional and the sagittal planes has two important roles. One is in the meridional direction to collect the needed information and to image the detected emission source on the meridional imaging plane as the subject for the grating. The second is to compensate the stigmatism in the sagittal direction of the concave grating. The flat-field concave grating also has the function to image besides the basic function as a dispersion component.

Parameters for the toroidal mirror and the flat-field concave grating in the spectrograph are symbolized and listed below in Table 1.

*Project supported by the National Natural Science Foundation of China (Grant Nos. 11221002, 11274152, and 11074297).

†Corresponding author. E-mail: qldong@aphy.iphy.ac.cn

© 2014 Chinese Physical Society and IOP Publishing Ltd

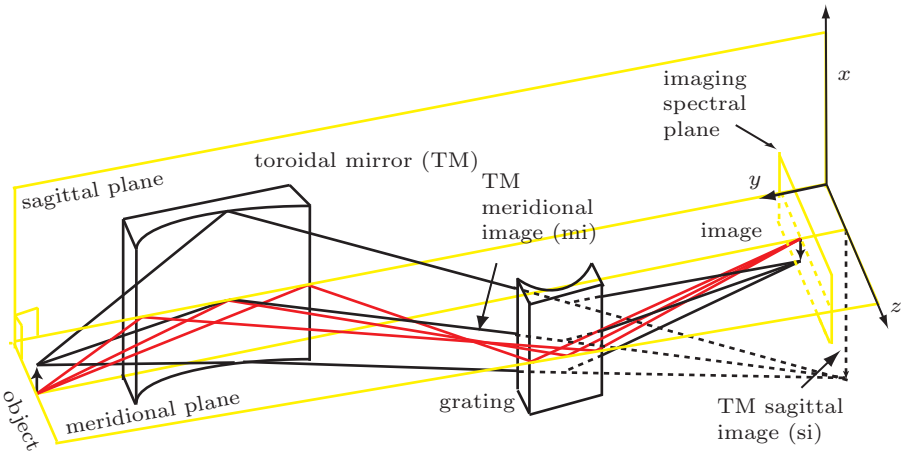


Fig. 1. (color online) Configuration of the flat-field spectrograph system consisting of a toroidal mirror and a varied line-spacing concave grating.

Table 1. Parameters for the toroidal mirror and flat-field concave grating in the spectrograph.

Toroidal mirror:	
Meridional radius of curvature	$r_t = 5194\pm$ mm
Sagittal radius of curvature	$\rho_s = 47.6$ mm
Incidence angle	$\alpha_1 = 86.3^\circ$
Distance of the source to the mirror	$l_{s2t} = 816.9$ mm
Distance of the meridional focus from the mirror	$l'_{t2mi} = 208$ mm
Distance of the sagittal focus from the mirror	$l'_{t2si} = l'_{t2mi} + l_{mi2g} + \mathrm{abs}(l'_{g2si})$ $= 208$ mm $+ 237$ mm $+ 240$ mm $= 685$ mm
Flat-field concave grating:	
Radius of curvature	$r_g = 5649$ mm
Distance of the meridional source from grating	$l_{mi2g} = 237$ mm
Distance of the spectral image from grating	$l'_{g2gi} = L/\sin\beta$
Normal Distance of the sagittal source from grating	$L = 235$ mm
Distance fo the sagittal source from grating	$l'_{g2si} = -240$ mm
Blaze angle	$\theta_B = 3.2^\circ$
Incidence angle	$\alpha_2 = 87^\circ$
Grating manufacture coefficients	$b_2 = -20$
	$b_3 = 4.558 \times 10^2$
	$b_4 = -1.184 \times 10^4$
	$\sigma_0 = 1/1200$ mm

For the alignment of the flat-field soft X-ray spectrometer, one can use the basic relationships among various distances to locate each component as listed below

Toroidal meridional:

$$\frac{1}{l_{s2t}} + \frac{1}{l'_{t2mi}} = \frac{2}{r_t \cos\alpha_1};$$

Toroidal sagittal:

$$\frac{1}{l_{s2t}} + \frac{1}{l'_{t2si}} = \frac{2\cos\alpha_1}{\rho_s};$$

Flat-field concave grating:

$$\frac{1}{l'_{g2si}} + \frac{1}{l'_{g2gi}} = \frac{\cos\alpha_2 + \cos\beta_2}{r_g};$$

$$l'_{t2mi} + l_{mi2g} + \mathrm{abs}(l'_{g2si}) = l'_{t2si}.$$

3. Formulas and calculated spectral images of optical components

3.1. Toroidal mirror

The toroidal surface is

$$z = r_t - r_t\left[1 - \frac{x^2+y^2}{r_t^2} + \frac{2\rho_s}{r_t}\left(\frac{\rho_s}{r_t} - 1\right)\left(1 - \sqrt{1 - \frac{x^2}{\rho_s^2}}\right)\right]^{1/2},$$

where r_t and ρ_s are the radii of the meridional and the sagittal planes, respectively. Usually, one expands the above expression in the field or pupil coordinates for analytical purpose. However, we would like to resolve numerically the intersections between lines and surfaces. The normal direction of the toroidal surface at point (x,y,z) is $N_x = -z_x/d$, $N_y = -z_y/d$,

and $N_z = z_z/d = 1/d$, with

$$
\begin{aligned}
z_x &= -r_\mathrm{t}\frac{-\dfrac{2x}{r_\mathrm{t}^2}+\dfrac{2\rho_\mathrm{s}}{r_\mathrm{t}}\left(\dfrac{\rho_\mathrm{s}}{r_\mathrm{t}}-1\right)\left(-\dfrac{-2x/\rho_\mathrm{s}^2}{2\sqrt{1-x^2/\rho_\mathrm{s}^2}}\right)}{2t},\\
z_y &= -r_\mathrm{t}\frac{-2y/r_\mathrm{t}^2}{2t},\\
t &= \sqrt{1-\frac{x^2+y^2}{r_\mathrm{t}^2}+\frac{2\rho_\mathrm{s}}{r_\mathrm{t}}\left(\frac{\rho_\mathrm{s}}{r_\mathrm{t}}-1\right)\left(1-\sqrt{1-\frac{x^2}{\rho_\mathrm{s}^2}}\right)},\\
d &= \sqrt{z_x^2+z_y^2+1}.
\end{aligned}
$$

If the incident ray is assumed to be represented by vector $\boldsymbol{I}$, and reflected at the point with normal $\boldsymbol{N}$, the reflected ray is then written as $\boldsymbol{R} = \boldsymbol{I} - 2(\boldsymbol{I}\cdot\boldsymbol{N})\boldsymbol{N}$.

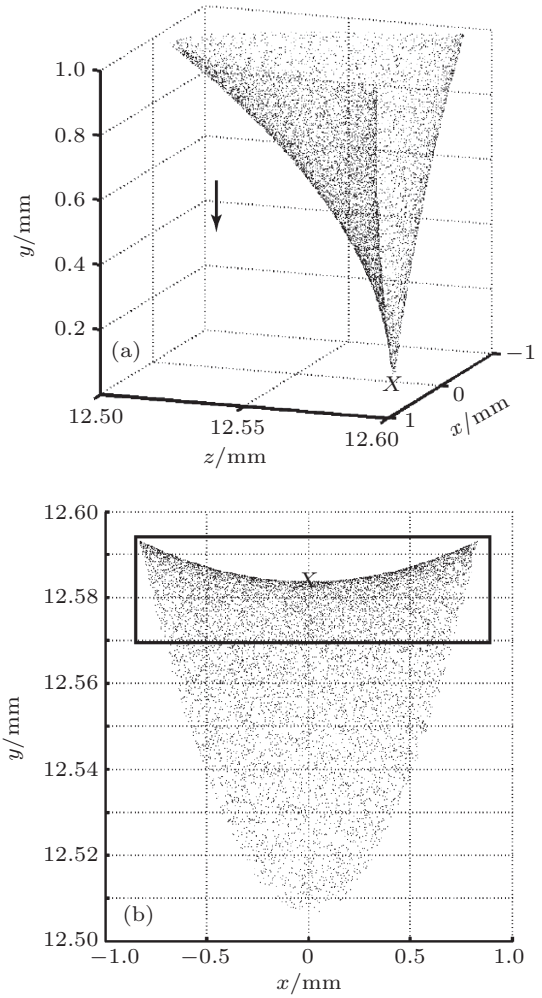


Fig. 2. Images of a single point source in the meridional plane of the toroidal mirror: (a) 3D images near the ideal imageing plane, (b) 2D images on the meridional focal plane.

Figure 2(a) shows the three-dimensional (3D) image of a point source in the meridional plane. The image point marked by "X" is the position of the intersection between the meridional image plane and the light along the principal axis of the spectrograph system. The other image points are the end positions of the off-axis light with the optical path equal to that of the on-axis ray. All the intersection points of the rays from the single point source with the imaging plane form the shape of a crescent moon, as shown in Fig. 2(b). To act as the object of the concave flat-field grating, a narrow slit with a width of tens of micrometers is usually used to select the good part of the signal, as indicated by the rectangle. The narrow slit is important in experiments mostly because the mirror is not an ideal toroidal surface and the badly reflected rays need to be removed. It is proven that the narrower slit helps to increase the spectral resolution significantly with a tolerated loss of signal flux.[5]

3.2. Aberration-corrected concave grating with varied line spaces

The used grating is manufactured mechanically by Hitachi, Ltd.[6] The relation between the groove number and the position is

$$n = \frac{1}{\sigma_0}\left(w_\theta + \frac{b_2}{r}w_\theta^2 + \frac{b_3}{r^2}w_\theta^3 + \frac{b_4}{r^3}w_\theta^4 + \cdots\right),$$

where $w_\theta = y - z\tan\theta$ with (x,y,z) on spherical surface $x^2 + y^2 + (z-r)^2 = r^2$. The groove numbers are expressed in this way because the groove patterns are curved if the grooves are projected onto the y–x plane. To express the patterns by parallel straight lines, the grooves are projected to the y–x plane from the θ direction, which is the tilt angle of the plane in which the tool reciprocation occurs. The patterns are basically determined by Fermat's principle, which requires the true optical path to be the shortest. Suppose the light starting from $A(x_\mathrm{s}, y_\mathrm{s}, z_\mathrm{s})$ and passing through $P(x,y,z)$ in the concave grating surface and arriving at image $A'(x_\mathrm{e}, y_\mathrm{e}, z_\mathrm{e})$, the light path function F can be expressed as $F = \langle AP\rangle + \langle PA'\rangle + nm\lambda$ and dealt with in various ways for different purposes. The light path function can be expanded as a power series of w_θ with complicated coefficients, as people usually do when in pursuit of the physical meanings. The light path function can also be resolved numerically if one is concerned about the images rather than the physical meanings.

3.2.1. Analytical expansion for the physical meanings

The light path function can be expanded as a power series of ω_θ with the terms

$$F_{ij} = C_{ij} + [m\lambda/\sigma_0]M_{ij}.$$

Each term corresponds to a correction of different orders of aberrations. To design an aberration-free spectrograph, all F_{ij} should be 0, which is impossible to satisfy. However, the main terms can be set to zero or a minimum value to reduce the aberrations. Physical meanings for the first several terms are F_{10}: dispersion grating; F_{20}: horizontal focal condition; F_{02}: astigmatism; F_{30}: coma-type aberration; others: high order aberrations.

The explicit expressions of c_{ij} and M_{ij} about the design of the aberration-corrected mechanically ruled concave grating can be found in the paper by Harada and Kita.[6] Only

some of them related to the above four coefficients are listed below

$$\begin{aligned} C_{10} &= -\sin\alpha - \sin\beta, \\ M_{10} &= 1, \\ C_{20} &= \frac{1}{2}\left(\frac{\cos^2\alpha}{l_{\mathrm{mi2g}}} - \frac{\cos\alpha}{r_{\mathrm{g}}}\right) + \frac{1}{2}\left(\frac{\cos^2\beta}{l'_{\mathrm{g2si}}} - \frac{\cos\beta}{r_{\mathrm{g}}}\right), \\ M_{20} &= \frac{1}{r_{\mathrm{g}}}\left(b_2 - \frac{\tan\theta}{2}\right), \end{aligned}$$

which comprise the relationships of the dispersion and the imaging of the grating

$$\begin{cases} \sigma_0(\sin\alpha + \sin\beta) = m\lambda, \\ -\dfrac{1}{2}\left(\dfrac{\cos^2\beta}{l'_{\mathrm{g2si}}} - \dfrac{\cos\beta}{r_{\mathrm{g}}}\right) \\ = \dfrac{1}{2}\left(\dfrac{\cos^2\alpha}{l_{\mathrm{mi2g}}} - \dfrac{\cos\alpha}{r_{\mathrm{g}}}\right) + \dfrac{1}{r_{\mathrm{g}}}\left(b_2 - \dfrac{\tan\theta}{2}\right)(m\lambda/\sigma_0). \end{cases}$$

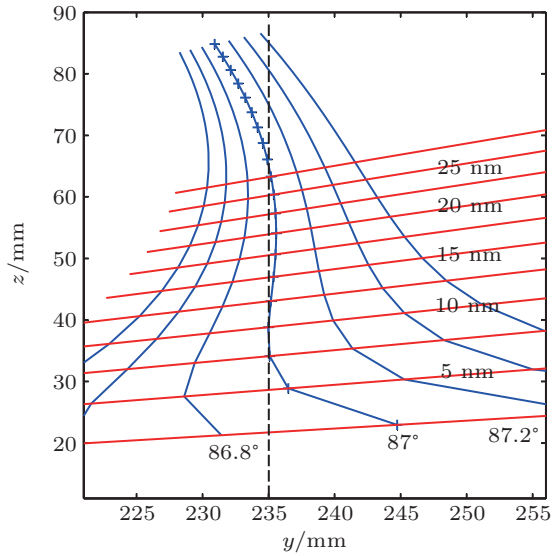


Fig. 3. (color online) Field characteristics of the varied ling-spacing grating for different incidence angles.

For a source point in the meridional plane, with the same incidence angle, signals with different wavelengths (λ) will form respective images with the corresponding distance l'_{g2si} and diffraction angle β to the grating. Figure 3 shows the image points of different wavelengths for different incidence angles. It is clear that the vertical plane at $y = 235$ mm is a good approximation of the real imaging plane. Other parameters such as b_2 are determined in the convenience of the grating manufacture also with considerations given to the flat-field formation.

3.2.2. Numerical resolution for more accurate images

By setting $M_{20} = -20/r_{\mathrm{g}}$, the groove number is then represented with w_θ replaced by y, and the light path function is rewritten as

$$F = \langle AP\rangle + \langle PA'\rangle + \frac{m\lambda}{\sigma_0}\left(y + \frac{b_2 y^2}{r} + \frac{b_3 y^3}{r^2} + \frac{b_4 y^4}{r^3} + \cdots\right).$$

Fermat's principle requires

$$\begin{cases} \dfrac{\partial F}{\partial x} = 0, \\ \dfrac{\partial F}{\partial y} = 0, \end{cases}$$

producing the reflected/diffracted ray with the cosine direction as follows:

$$\begin{cases} R_x = xQ - I_x, \\ R_y = yQ - (I_y + mf\lambda/\sigma_0), \\ R_z = (z-r)Q - I_z, \end{cases}$$

where Q is defined as

$$Q = -\frac{1}{r}\left\{\cos I - \frac{myf\lambda}{r\sigma_0} + \left[\left(\cos I - \frac{myf\lambda}{r\sigma_0}\right)^2 - \left(\frac{2mf\lambda I_y}{\sigma_0} + \frac{m^2 f^2\lambda^2}{\sigma_0^2}\right)\right]^{1/2}\right\},$$

and f is introduced here as

$$f = \sigma_0\frac{\partial n}{\partial y} = \left(1 + \frac{2b_2 y}{r} + \frac{3b_3 y^2}{r^2} + \frac{4b_4 y^3}{r^3}\right).$$

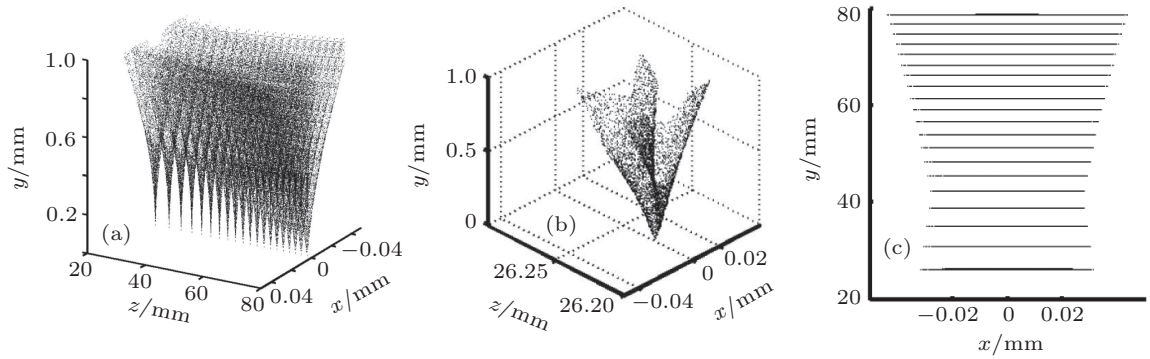


Fig. 4. Spectral images of a single point source by the flat-field grating: (a) 3D spectral images near the flat-field plane, (b) 3D image at the wavelength of 2.5 nm, (c) 2D images on the flat spectral plane of the grating.

Figure 4(a) is the 3D multi-wavelength image of a single point source in the meridional plane, 237 mm away from the apex of the grating. The $\delta y = 0$ indicates the vertical plane at $y = 235$ mm. Figure 4(b) gives the detailed image at the wavelength of 2.5 nm. The two-dimensional (2D) image of a single point emitting various wavelengths is given in Fig. 4(c). As the grating is astigmatism-optimized at 10 nm, the length in the x direction of the image around 10 nm is evidently shorter than that at other wavelengths.

4. Comparison of the spectral images obtained by calculations and experiments

The flat-field spectrograph system is designed and assembled by assuming that the basic equations between various distances are satisfied. However, the always existing error in the instrument alignment can cause deviations of the actual spectral images from theoretical calculations. There are some experimental parameters that can be changed within specific ranges without causing large variations of the spectral image characteristics. For example, when the light source has a volume less than 1500 μm × 20000 μm × 80 μm in the (x, y, z) coordinates, the change of the spectral resolution is negligible.[5] In some cases, the changes of one parameter can be compensated by the corresponding changes of another parameter. For example, the object distance of the grating can be changed together with the grazing incidence angle while the actual spectral surface can still be well approximated by a plane.[7]

In the actual alignment and application of the flat-field spectrograph system, people might encounter various kinds of deviations of the spectral images from the theoretical ones. We present the deviation example when the image recording surface is not precisely located on the flat imaging plane of the varied line-spacing concave grating. The experimental results for the case in which the charge coupled device (CCD) surface is off the flat-field plane are also given as a comparison to the spectra obtained by the well aligned spectrometer.

Figure 5 shows the calculated spectral images when the charge coupled device recorder surface is or is not located on the flat-field plane of the grating. When the charge coupled device recorder surface is precisely located on the grating's flat spectral plane, the spectral image of one single point source in the meridional plane is continuous (Fig. 5(a)). When the charge coupled device surface is off the flat spectral plane, however, the image is broken into two parts, together with the deterioration of the spectral resolution (Fig. 5(b)). The characteristic change caused by the relative location of the recorder surface with respect to the flat-field spectral plane of the grating can be verified with experimental results. When all optical components are located on the expected positions, the laser plasma is correctly imaged on the charge coupled device surface with good spatial and spectral resolutions. However, if the charge coupled device recording surface is off the flat spectral plane of the grating, the recorded spectral image breaks into two parts as the numerical calculation predicts.[8,9]

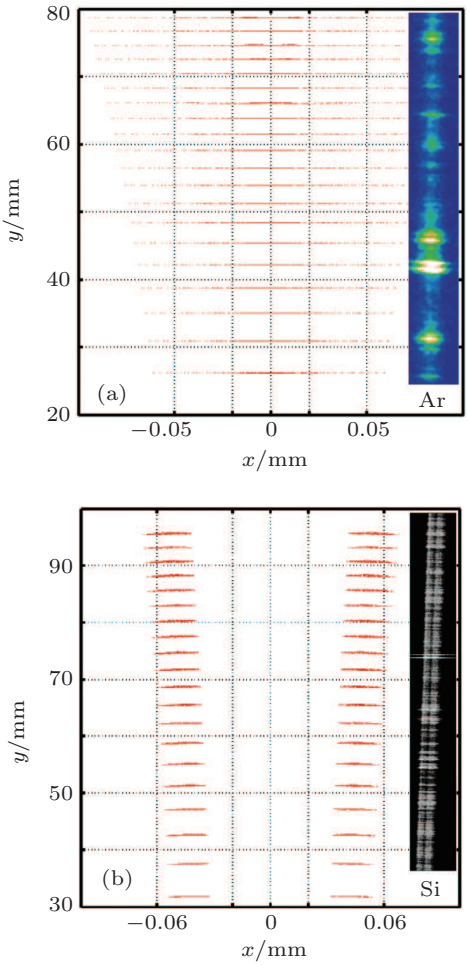


Fig. 5. (color online) The spectral images of a single point source in the meridional plane of the flat-field spectrograph system consisting of a toroidal mirror and a concave grating with varied line spaces: (a) the situation with the spectrometer well aligned, (b) the situation with the recorder surface off the flat spectral plane of the grating. Experimental results for the two corresponding cases are given as insets for comparison.

5. Summary

The ray-tracing method is introduced for helping alignment and spectra analysis of the soft X-ray spectrograph system consisting of a toroidal mirror, a slit, and a flat-field concave grating with varied line spaces. The necessary formulas are derived and can be applied in the numerical code capable of producing images of every component in the system.

These images can be compared to the experimental results, so researchers can have a reference during the instrument alignment and the experimental data analysis.

References

[1] Harada T and Kita T 1980 *Appl. Opt.* **19** 3987

[2] Chrisp M P 1983 *Appl. Opt.* **22** 1508

[3] Li R X, Fan P Z, Xu Z Z, Zhang Z Q and Lu P X 1994 *Opt. Eng.* **33** 2366

[4] Choi W, Lee J U and Nam C H 1997 *Appl. Opt.* **36** 1457

[5] Liu Y Q, Zhang J, Chen Z L and Peng X Y 2004 *Acta Phys. Sin.* **53** 1433 (in Chinese)

[6] Kita T, Harada T, Nakano N and Kuroda H 1983 *Appl. Opt.* **22** 512

[7] Li Y J, Yang J L and Zhang J 2000 *Acta Phys. Sin.* **49** 863 (in Chinese)

[8] Liang G Y, Zhao G, Zhong J Y, Li Y T, Liu Y Q, Dong Q L, Yuan X H, Jin Z and Zhang J 2008 *ApJSS* **177** 326

[9] Liu Y Q, Dong Q L, Peng X Y, Jin Z and Zhang J 2009 *Phys. Plasmas* **16** 043301